Research Square

Preprints are preliminary reports that have not undergone peer review.
They should not be considered conclusive, used to inform clinical practice,
or referenced by the media as validated information.

Unlocking the Antibacterial and Anti-Biofilm Potential of Otostegia fruticosa Phenolics Against Pseudomonas aeruginosa: Confocal Imaging and Molecular Docking Evidence

Gadah A. Al-Hamoud
King Saud University
Basmah Almaarik
King Saud University
Ayesha Mateen
amateen.c@ksu.edu.sa
King Saud University
Musarat Amina
King Saud University

Article

Keywords: Otostegia fruticosa, Psoralen, Galetin 3,6-dimethyl ether, P. aeruginosa, Antibacterial, Anti-Biofilm, Molecular docking

Posted Date: November 13th, 2026

DOI: https://doi.org/10.21203/rs.3.rs-11376957/v1

License: This work is licensed under a Creative Commons Attribution 4.0 International License.
Read Full License

Additional Declarations: No competing interests reported.

Unlocking the Antibacterial and Anti-Biofilm Potential of *Otostegia fruticosa* Phenolics Against *Pseudomonas aeruginosa*: Confocal Imaging and Molecular Docking Evidence

Gadah A. Al-Hamoud[1], Basmah Almaarik[2], Ayesha Mateen[2*], Musarat Amina[1*]
galhamoud@ksu.edu.sa , balmaarik@ksu.edu.sa , amateen.c@ksu.edu.sa, mamina@ksu.edu.sa ,

[1]Department of Pharmacognosy, College of Pharmacy, King Saud University, Riyadh 11495, P.O. Box 22452, Saudi Arabia

[2]Department of Clinical Laboratory Science, College of Applied Medical Sciences, King Saud University, Riyadh 12371, Saudi Arabia

*Correspondence should be addressed to Ayesha Mateen, amateen.c@ksu.edu.sa
Musarat Amina, mamina@ksu.edu.sa

Abstract

Pseudomonas aeruginosa is an opportunistic pathogen characterized by intrinsic antimicrobial resistance, extensive virulence, and persistent biofilm formation. This study evaluated the antibacterial, antibiofilm, and quorum-sensing-targeting potential of psoralen and galetin 3,6-dimethyl ether isolated from *Otostegia fruticosa*. Minimum inhibitory concentrations (MIC) and MTT reduction assays revealed strong antibacterial activity, with galetin 3,6-dimethyl ether exhibiting an MIC of 125 µg/mL (96.83% growth inhibition) and psoralen showing an MIC of 175µg/mL (98.93% inhibition). Confocal laser scanning microscopy demonstrated marked structural disruption of mature biofilms: psoralen reduced green and red fluorescence intensities by 92.4% and 84.1%, respectively, and decreased mean biofilm thickness from 98 ± 2.00 µm to 83.00 ± 2.00 µm , whereas galetin 3,6-dimethyl ether reduced green and red fluorescence by 82.4% and 91.7%, respectively. Molecular docking predicted favorable binding interactions with quorum-sensing regulators, yielding docking scores of -7.47 kcal/mol for psoralen with LasR and -6.94 kcal/mol for galetin 3,6-dimethyl ether with RhlR. These specific findings establish both phytochemicals as promising natural antibacterial and antibiofilm lead compounds against P. *aeruginosa.*

Keywords *Otostegia fruticosa*· Psoralen· Galetin 3,6-dimethyl ether· *P. aeruginosa*· Antibacterial· Anti-Biofilm· Molecular docking

Introduction

Bacterial resistance has emerged as one of the most critical global public health challenges of the 21st century, severely compromising the efficacy of standard antibiotic therapies and threatening modern medical procedures[1]. The rapid rise of multidrug-resistant (MDR) pathogens has significantly reduced the utility of conventional therapeutics, resulting in prolonged hospitalizations, escalating healthcare costs, and elevated morbidity and mortality rates worldwide[2]. Within this landscape of escalating antimicrobial resistance, *Pseudomonas aeruginosa* stands out as a pathogen of primary concern due to its remarkable adaptability, intrinsic resistance mechanisms, and ability to survive in diverse environmental and clinical niches[3].

Pseudomonas aeruginosa is a Gram-negative, opportunistic human pathogen whose clinical significance is driven by extensive metabolic versatility, a formidable array of virulence factors, and an exceptional capacity to acquire resistance to multiple antimicrobial agents[4,5]. Consequently, it represents a leading cause of severe healthcare-associated infections, including hospital-acquired pneumonia, urinary tract infections, burn wound colonization, bloodstream infections, and chronic respiratory decline in immunocompromised patients[6]. The pathogenicity of *P. aeruginosa* is mediated by an extensive arsenal of virulence determinants, such as exotoxins, elastases, proteases, pyocyanin, rhamnolipids, and sophisticated quorum-sensing (QS) systems that regulate bacterial communication, host colonization, and biofilm maturation[7]. These virulence factors collectively enable the bacterium to evade host immune defenses, adapt to hostile microenvironments, and persist despite intensive antimicrobial intervention.

The clinical persistence of *P. aeruginosa* is heavily driven by its propensity to transition from a free-floating planktonic state into a sessile, biofilm-associated community[8]. Biofilm-associated infections are notoriously recalcitrant to therapy; embedded bacterial cells exhibit up to a 1,000-fold increase in resistance to antibiotics, disinfectants, and host immune defenses compared to their planktonic counterparts [9]. The biofilm matrix, composed primarily of extracellular polymeric substances (EPS), acts as a diffusion barrier that restricts antibiotic penetration and promotes metabolic dormancy[10]. Furthermore, *P. aeruginosa* frequently participates in polymicrobial biofilms, where synergistic interactions with co-infecting microorganisms enhance community stability and virulence[11]. Such biofilm-mediated consortia severely complicate the management of chronic conditions, including non-healing surgical wounds, diabetic foot ulcers, and persistent pulmonary infections in cystic fibrosis patients[12].

The alarming prevalence of MDR *P. aeruginosa* strains has severely restricted therapeutic options, underscoring the urgent need for novel anti-infective paradigms. In this context, plant-derived bioactive compounds have attracted considerable attention owing to their chemical diversity, favorable biocompatibility, and unique multi-target mechanisms that minimize the selective pressure driving resistance[13]. Numerous phytochemicals and essential oils have demonstrated promising antibacterial and antibiofilm efficacy against critical priority pathogens such as *P. aeruginosa*, *Staphylococcus aureus*, *Escherichia coli*, *Klebsiella pneumoniae*, and *Acinetobacter baumannii*, positioning them as promising templates for next-generation antimicrobial agents.

Among medicinal plants of the *Lamiaceae* family, *Otostegia fruticosa* (Forssk.) Schweinf. ex Penz. is an aromatic shrub widely distributed across the Horn of Africa and the Arabian Peninsula. In traditional medicine, this species has long been employed for wound cleansing and the management of infectious and inflammatory disorders[14]. Pharmacological evaluations of *O.*

fruticosa extracts have validated these ethnobotanical applications, demonstrating broad-spectrum bioactivities, including antimicrobial, antioxidant, antiparasitic, and anticancer properties[15–17]. Phytochemical profiling attributes these therapeutic effects to a rich variety of secondary metabolites, predominantly diterpenoids, coumarins, and flavonoids[17].

Among these bioactive constituents, two specific phenolic compounds; psoralen and galetin 3,6-dimethyl ether are of particular pharmacological interest. Psoralen (7H-furo[3,2-g]chromen-7-one) is a linear furanocoumarin comprising a coumarin nucleus fused to a furan ring[18]. It possesses well-documented antioxidant, antimicrobial, antiviral, anti-inflammatory, and antitumor activities, and is clinically administered alongside ultraviolet-A radiation (PUVA therapy) to manage refractory dermatological conditions such as psoriasis, vitiligo, and eczema[19,20]. Concurrently, galetin 3,6-dimethyl ether, a methoxylated flavonoid, exhibits pronounced anti-inflammatory, spasmolytic, and tocolytic properties[21-23], which are primarily mediated through calcium channel blockade and potassium channel activation.

Despite the individual therapeutic significance and broad botanical occurrence of these two secondary metabolites, their presence in and specific contributions to the bioactivity of *O. fruticosa* remain insufficiently investigated. To address this knowledge gap, psoralen (**1**) and galetin 3,6-dimethyl ether (**2**) were isolated and purified from the aerial parts of *O. fruticosa*. The primary objective of this study was to evaluate their antibacterial and antibiofilm efficacy against *Pseudomonas aeruginosa* (ATCC 27853). To complement these empirical findings, molecular docking simulations targeting the LasR and RhlR quorum-sensing transcriptional regulators were performed to gain mechanistic insights into their potential modes of action against bacterial communication pathways. Additionally, their radical-scavenging capacity was assessed using the 2,2-diphenyl-1-picrylhydrazyl (DPPH) assay.

Materials and methods

Plant material

The aerial parts (stems and leaves) of *Otostegia fruticosa* Forssk. were collected at the pre-flowering stage from the Medicinal Plants Garden, Department of Pharmacognosy, College of Pharmacy, King Saud University, Riyadh, Saudi Arabia, in April 2020. The plant material was authenticated by comparison with a reference voucher specimen deposited in the departmental herbarium (Voucher No. 15312). The collected plant material was air-dried in the shade at ambient temperature, ground into a coarse powder, and 1 kg of the powdered material was subjected to phytochemical investigation and compound isolation.

Extraction and isolation

The pulverized, shade-dried aerial parts of *O. fruticosa* (500 g) were initially subjected to cold percolation with petroleum ether (1.0 L) at room temperature to eliminate lipophilic components and pigments. The resulting defatted plant residue (470 g) was subsequently extracted by exhaustive maceration with 95% methanol (4×1.0 L) for 72 h per cycle at ambient temperature. The combined menstrua were filtered and evaporated to dryness under reduced pressure at 50 ± 2 ◦C using a rotary evaporator. The remaining aqueous residue was lyophilized to yield 80.5 g of crude amorphous methanolic extract. Preliminary biological screening demonstrated that the crude methanolic extract possessed significant antibacterial activity. To localize and concentrate the active constituents, the crude extract was suspended in distilled water (200 mL) and subjected to sequential liquid-liquid partitioning with organic solvents of increasing polarity, yielding the dichloromethane (CH_2Cl_2, 45.3 g), ethyl acetate (EtOAc, 14.26 g), and n-butanol (BuOH, 8.21 g) and residual aqueous (23.2 g) fraction. Comparative thin-layer chromatography (TLC) and

phytochemical profiling indicated that the CH_2Cl_2 fraction was markedly enriched in phenolic secondary metabolites and was therefore selected for detailed chromatographic isolation.

Isolation and purification of bioactive compounds 1 and 2

A portion of the CH_2Cl_2-soluble fraction (40.0 g) was loaded onto a silica gel column (60–120 mesh, 100 × 5 cm) for normal-phase column chromatography. Gradient elution was performed starting with n-hexane, progressing through pure CH_2Cl_2, and incrementally increasing polarity with methanol (CH_2Cl_2-MeOH, 100: 0→ 0: 100 v/v) to yield four major pooled fractions (Fr.1-4). Fraction Fr-1, eluted with 10% MeOH in CH_2Cl_2 showed an identical TLC pattern (run in CHCl3: MeOH::98:2) with one major spot having R_f value of 0.26 visualized by freshly prepared Borinate-PEG spray reagent (2-aminoethyl diphenylborinate, 1% in methanol: polyethylene glycol-4000, 5% ethanol, 1:1, v/v). Combined subfractions displaying identical TLC characteristics were pooled and concentrated under reduced pressure. This Fraction (Fr-1, 8.7 mg) was further purified by preparative reversed-phase HPLC using a CH_3CN–H_2O gradient system to yield compound **1** (19.9 mg). Fraction Fr-4 obtained by elution with 20% MeOH in CH_2Cl_2 displayed a consistent TLC profile (run in $CHCl_3$: MeOH::17:3) characterized by a prominent spot (R_f = 0.28) visualized by freshly prepared vanillin boric acid reagent. Subfractions exhibiting identical TLC profiles were pooled, concentrated under reduced pressure, and recrystallized from MeOH to afford a white amorphous powder (3.5 g, compound **2**). The isolation and purification procedures for compounds **1** and **2** were performed according to methods previously reported by our group. The structures of the purified compounds were established by comprehensive spectroscopic analyses, including 1D and 2D and HRMS spectra, and were further confirmed by comparison of their spectroscopic data with those reported in the literature [24, 25].

Identification of compounds 1 and 2

Compound **1** was obtained as colourless needle-shaped crystals, mp 160–165 °C. HRMS exhibited a molecular ion peak at *m/z* 187.0399 $[M+H]^+$, consistent with the calculated value for $C_{11}H_7O_3$ (*m/z* 187.0395). The ^{1}H-NMR (400 MHZ, $CDCl_3$) showed resonances at *δ*: 6.41(1H, *d*, *J* = 9.6 Hz, 3-H), 6.86 (1H, *d*, *J* = 1.2 Hz, 3'-H), 7.50 (1H, *s*, 8-H), 7.82 (1H, *d*, *J* = 1. 2 Hz, 2'-H), 7.82 (1H, *d*, *J* = 9.6 Hz, 4-H). The ^{13}C-NMR (150 MHz, $CDCl_3$) displayed signals at *δ*: 161.0 (C-2), 156.4 (C-7), 152.0 (C-9), 146.9 (C-2'), 144.0 (C-4), 124.8 (C-6), 119.8 (C-5), 115.4 (C-10), 114.6 (C-3), 106.4 (C-3'), 99.9 (C-8). The spectroscopic data obtained are consistent with psoralen reported in the literature[26], confirming the identity of compound **1**.

Compound **2**: Compound **2** was obtained as a yellow amorphous solid, mp. 217-225 °C. HRMS (ESI) showed an ion at *m/z* 329.0677 $[M-H]^-$ (calcd for $C_{17}H_{13}O_7^-$, 329.0661) and an ion at *m/z* 331.0825 $[M+H]^+$ (calcd for $C_{17}H_{15}O_7^+$, 331.0817). The ^{1}H-NMR (400 MHZ, DMSO-d_6) showed resonances at *δ*: 7.94 (2H, *d*, *J* = 9.0, H-2'/6'), 6.52 (2H, *d*, *J* = 9.0, H-3'/5'), 3.78 (3H, *s*, -OMe), 3.75 (3H, *s*, -OMe). The ^{13}C-NMR (150 MHz, DMSO-d_6) displayed signals at *δ*: 160.6 (C-2), 178.53 (C-4), 156.0 (C-5), 152.7 (C-9), 152.1 (C-4'), 137.7 (C-3), 131.7 (C-6), 130.6 (C-2'/6'), 121.0 (C-1'), 116.1 (C-3'/5'), 104.8 (C-10), 94.5 (C-8), 60.3 (C-OMe), 60.1 (C-OMe). Comparison of these spectroscopic data with those reported in the literature supported the identification of compound **2** as 5,7,4′-trihydroxy-3,6-dimethoxyflavone (Galetin 3,6-dimethyl ether) [25].

Antibacterial activity

Bacterial strain and culture preparation

A reference strain of *Pseudomonas aeruginosa* (ATCC 27853) was used in this study. The bacterium was cultured on Mueller–Hinton agar (MHA) and incubated at 37°C for 18–24 h. A single well-isolated colony was transferred into Mueller–Hinton broth (MHB) and incubated overnight at 37°C under aerobic conditions. The bacterial suspension was adjusted to a turbidity

equivalent to a 0.5 McFarland standard (approximately 1.5×10^8 CFU/mL) and subsequently diluted in MHB to obtain a final inoculum concentration of approximately 5×10^5 CFU/mL for susceptibility testing, in accordance with the Clinical and Laboratory Standards Institute (CLSI)

Determination of minimum inhibitory concentration (MIC)

The minimum inhibitory concentrations (MICs) of compound **1** and compound **2** against *P. aeruginosa* (ATCC 27853) were determined using the broth microdilution method in sterile 96-well microtiter plates following CLSI guidelines (CLSI, 2025). Briefly, two-fold serial dilutions of each test compound were prepared in Mueller–Hinton broth. Subsequently, an equal volume of the standardized bacterial inoculum was added to each well to achieve a final bacterial concentration of approximately 5×10^5 CFU/mL. Wells containing inoculated broth without test compounds served as growth controls, whereas wells containing only sterile broth served as sterility controls. The microplates were incubated at 37°C for 24 h. Following incubation, bacterial viability was assessed using the MTT colorimetric assay. Briefly, 40 µL of MTT solution [3-(4,5-dimethylthiazol-2-yl)-2,5-diphenyltetrazolium bromide; 5 mg/mL in DMSO] was added to each well, and the plates were further incubated at 37°C for 2–4 h. Metabolically active bacterial cells reduced the yellow tetrazolium salt to insoluble purple formazan crystals, indicating cellular viability. The absorbance was measured at 600 nm using a microplate reader. The MIC was defined as the lowest concentration of the test compound that completely inhibited bacterial growth, as evidenced by the absence of visible color development and metabolic activity relative to the growth control[27]. Percentage inhibition was calculated using the following equation.

$$\text{Growth Inhibition percentage (\%)} = \left(\frac{\mathrm{OD_{control}} - \mathrm{OD_{treated}}}{\mathrm{OD_{control}}}\right) \times 100$$

Assessment of outer membrane permeabilities and cellular leakage

The membrane-disruptive effects of Compounds **1** and **2** against *P. aeruginosa* were determined by quantifying the extracellular release of intracellular UV-absorbing biomolecules (nucleic acids and proteins), following previously described methods[28], with minor modifications. Exponential-phase *P. aeruginosa* cultures were treated with increasing concentrations of Compound **1** (125 µg/mL) and Compound **2** (175 µg/mL) at their respective MIC values. Untreated bacterial suspensions served as negative controls to determine baseline spontaneous lysis, while untreated cultures lysed via sonication or detergent treatment served as positive controls. Following incubation at 37 °C for 24 h under aerobic conditions, the cell suspensions were harvested and centrifuged at 13,000 × g for 5 min at 4 °C to yield cell-free supernatants. The extracellular concentrations of leaked nucleic acids and proteins were determined spectrophotometrically by measuring absorbance at 260 nm (A_{260}) and 280 nm (A_{280}), respectively, using a NanoDrop 8000 spectrophotometer (Thermo Fisher Scientific, USA). All assays were performed in technical triplicate across three independent biological replicates (n = 3). Results were background-corrected against compound-only blank controls in MHB and expressed as mean ± standard deviation (SD). Statistical differences compared to untreated controls were evaluated using one-way analysis of variance (ANOVA) followed by Dunnett's post-hoc test ($p < 0.05$).

Biofilm Viability Analysis

The effect of compound **1** and compound **2** on *P. aeruginosa* biofilm architecture and cell membrane integrity was evaluated using the LIVE/DEAD™ BacLight™ Bacterial Viability Kit (Thermo Fisher Scientific, Waltham, MA, USA). *P. aeruginosa* biofilms were established in sterile 8-well glass-bottomed chamber slides (ibidi GmbH, Gräfelfing, Germany) by seeding 200 µL of bacterial suspension (~1×10^5 CFU/mL in Mueller–Hinton broth) per well and incubating statically for 24 h at 37°C. Pre-established biofilms were carefully washed three times with sterile 0.01 M

phosphate-buffered saline (PBS; pH 7.4) to remove non-adherent and planktonic cells. Biofilms were then exposed to media containing compound **1** (175 μg/mL), compound **2** (125 μg/mL) or vehicle control (0.1\% v/v DMSO in PBS) for an additional for 24 h at 37°C. Untreated biofilms were maintained as controls. Following treatment, supernatants were aspirated, and the biofilms were gently washed twice with sterile 0.9% w/v NaCl. The dual-staining working solution was prepared by diluting 3 μL of SYTO 9 (3.34 mM in DMSO) and 3 μLof propidium iodide (PI; 20mM in DMSO) per 1mL of sterile 0.9% NaCl. Aliquots of 150 μL of staining cocktail were added to each chamber well and incubated for 20 min at room temperature (22-25 °C) in the dark. Excess stains were removed by washing once with 0.9% NaCl. Fluorescence imaging was performed using a Confocal Laser Scanning Microscope equipped with a × 63 oil-immersion objective lens. SYTO 9 fluorophore (membrane-permeant; labeling intact green live cells) was excited at 488 nm and collected at 500-540 nm. Propidium iodide (membrane-impermeant; labeling compromised red dead cells) was excited at 561 nm and collected at 600-650 nm. Optical z-sections (z-stacks) were acquired sequentially along the vertical axis at step intervals of 0.5-1.0 μm across at least five randomly chosen microscopic fields per sample replicate[29].

Quantitative Image Processing and Anti-Quorum Sensing Structural Analysis

To quantify the compound-mediated disruption of quorum sensing-dependent biofilm architecture, three-dimensional (3D) stack models and maximum-intensity projection (XY-plane view) images were reconstructed and analyzed using ImageJ/FIJI software (NIH, Bethesda, MD, USA) paired with COMSTAT 2. Spatial and architectural metrics indicative of anti-quorum sensing activity, including green-to-red integrated fluorescence intensity ratios (FI_{green}/FI_{red} for cell viability), mean biofilm thickness (μm), biomass volume ($\mu m^3/\ \mu m^2$), and substratum surface coverage (%) were calculated across at least five randomly selected, equalized regions of interest (ROIs) per sample[30].

All images were acquired under identical laser power, detector gain, and offset configurations to ensure unbiased comparative quantification, with data collected from three independent biological replicates (n = 3) and expressed as mean ± standard deviation.

Molecular Docking

To evaluate the binding interactions of the test compounds (**1** and **2**) against key quorum-sensing (QS) transcriptional regulators in *P. aeruginosa*, molecular docking simulations were conducted targeting the RhlR and LasR proteins. These proteins are central components of the RhlR and LasR quorum-sensing systems, respectively, and regulate the expression of numerous genes associated with virulence factor production, biofilm development, motility, and bacterial cell-to-cell communication. The three-dimensional crystal structures of the target proteins, RhlR (PDB ID: 8DQ1) and LasR (PDB ID: 3IX3), were retrieved from the Research Collaboratory for Structural Bioinformatics Protein Data Bank (RCSB PDB) in PDB format[31]. Azithromycin (PubChem CID: 447043), used as a reference anti-quorum sensing compound, was obtained from the PubChem database in SDF format. The chemical structures of psoralen and Galetin 3,6-dimethyl ether were drawn using ChemDraw and exported as MOL files. Subsequently, all ligand structures were converted to PDB format using Open Babel version 2.4.1[32]. To obtain energetically favorable conformations, ligand geometries were subjected to energy minimization using Avogadro software before docking analysis[33, 34].

Protein preparation was performed using AutoDock Tools (ADT) version 1.5.7. Briefly, crystallographic water molecules, co-crystallized ligands, and non-essential heteroatoms were removed from the protein structures. Polar hydrogen atoms were added, and Kollman united-atom partial charges were assigned to the receptors. The prepared protein structures were then saved in PDBQT format. Ligand preparation involved the addition of Gasteiger charges, merging non-polar

hydrogen atoms, assignment of rotatable bonds, and conversion to PDBQT format [35]. Molecular docking simulations were carried out using AutoDock version 4.2 employing the Lamarckian Genetic Algorithm (LGA). Grid boxes were defined to encompass the ligand-binding domains of the target proteins and were centered on the active-site regions to allow unrestricted ligand exploration within the binding pocket. Docking parameters were set to 100 independent runs, a population size of 150 individuals, a maximum of 2.5×10^6 energy evaluations, and 27,000 generations per run. The resulting docking conformations were clustered using a root-mean-square deviation (RMSD) tolerance of 2.0 Å. For each ligand–protein complex, the binding pose exhibiting the lowest predicted binding free energy and the most favorable intermolecular interactions within the active site was selected for further analysis. Binding affinities were expressed as docking scores (kcal/mol), and protein–ligand interactions, including hydrogen bonds, hydrophobic contacts, π–π interactions, and van der Waals interactions, were analyzed and visualized using Discovery Studio Visualizer version 24.1.0.23298. The docking results were subsequently compared with those of the reference compound azithromycin to evaluate the potential quorum-sensing inhibitory properties of the metabolites investigated.

Calculation of relative binding affinity (ΔΔG) and fold difference

Relative binding affinities of compound **1** (Psoralen) versus Azithromycin toward the LasR receptor, and compound **2** (Galetin 3,6-dimethyl ether) versus Azithromycin toward the RhlR receptor, were determined through a comparative analysis of docking-derived binding free energies (ΔG). To evaluate relative thermodynamic stabilization and active-site complementarity, the differential free energy ($\Delta\Delta G$) between each test ligand (A) and the reference ligand (B) was calculated as:

$$\Delta\Delta G = \Delta G_A - \Delta G_B \qquad \text{(i)}$$

where ΔG_A represents the docking binding free energy of the test compound (compound **1** or compound **2**), and ΔG_B represents the binding free energy of azithromycin within the same receptor system.

The calculated $\Delta\Delta G$ values were converted into relative changes in equilibrium dissociation/inhibition constants (K_d/K_i) using the thermodynamic relationship:

$$\Delta G = RT\ln K \qquad \text{(ii)}$$

where R is the universal gas constant (0.001987 kcal mol^{-1} K^{-1}) and T is the absolute temperature (298.15 K). Under these conditions, the value of RT = 0.592 kcal mol^{-1}.

The corresponding fold difference in binding affinity between the test and reference ligands was computed using the exponential Boltzmann relationship:

$$\text{Fold difference} = exp\left(\frac{\Delta\Delta G}{RT}\right) \qquad \text{(iii)}$$

where *exp* is the base of the natural logarithm (2.71828). This approach provides a quantitative estimate of the relative binding strength of the compounds compared with azithromycin within the same receptor environment. Because all ligands were docked against identical receptor structures using the same scoring function and computational protocol, the resulting ΔΔG values reflect relative thermodynamic stabilization and binding-site complementarity rather than absolute experimental affinity constants. The methodology was adopted according to established thermodynamic principles for interpreting docking-derived free energy differences and relative ligand binding affinities[36].

Statistical analysis

All results were expressed as the mean ± standard deviation (SD), based on triplicate measurements from three independent experiments. Statistical analyses were performed using GraphPad Prism version 9.2.0 (GraphPad Software, San Diego, CA, USA). Differences among

experimental groups were assessed by one-way analysis of variance (ANOVA), followed by Tukey's post hoc multiple-comparison test. A *p*-value below *0.05* was considered statistically significant.

Results and discussion

Phytochemical isolation and structural confirmation

Following preliminary screening, we selected the CH_2Cl_2-soluble fraction from the methanolic extract of the aerial parts of *O. fruticosa* for detailed phytochemical investigation. Sequential chromatographic fractionation of this fraction yielded two known phenolic constituents (compounds **1** and **2**; Fig. 1). Their structures were elucidated using comprehensive 1D and 2D NMR, including ^{1}H NMR, ^{13}C NMR, HSQC, and HMBC spectroscopy, along with HR-ESI-MS. Structural assignments were established by comparing the obtained spectroscopic data with previously reported literature values. Compound **1** was isolated as a crystalline solid and identified as psoralen (7H-furo[3,2-g]chromen-7-one), a linear furanocoumarin, consistent with previously reported data[26]. Compound **2** was identified as galetin 3,6-dimethyl ether (5,7,4′-trihydroxy-3,6-dimethoxyflavone), a methoxylated flavonoid, based on comparison with published spectroscopic data[25]. To the best of our knowledge, this study represents the first report of both compounds from the genus *Otostegia*, thereby expanding the chemotaxonomic knowledge of *O. fruticosa*. The 1D and 2D NMR spectra of both compounds are provided in the Supplementary Information (Fig. S1).

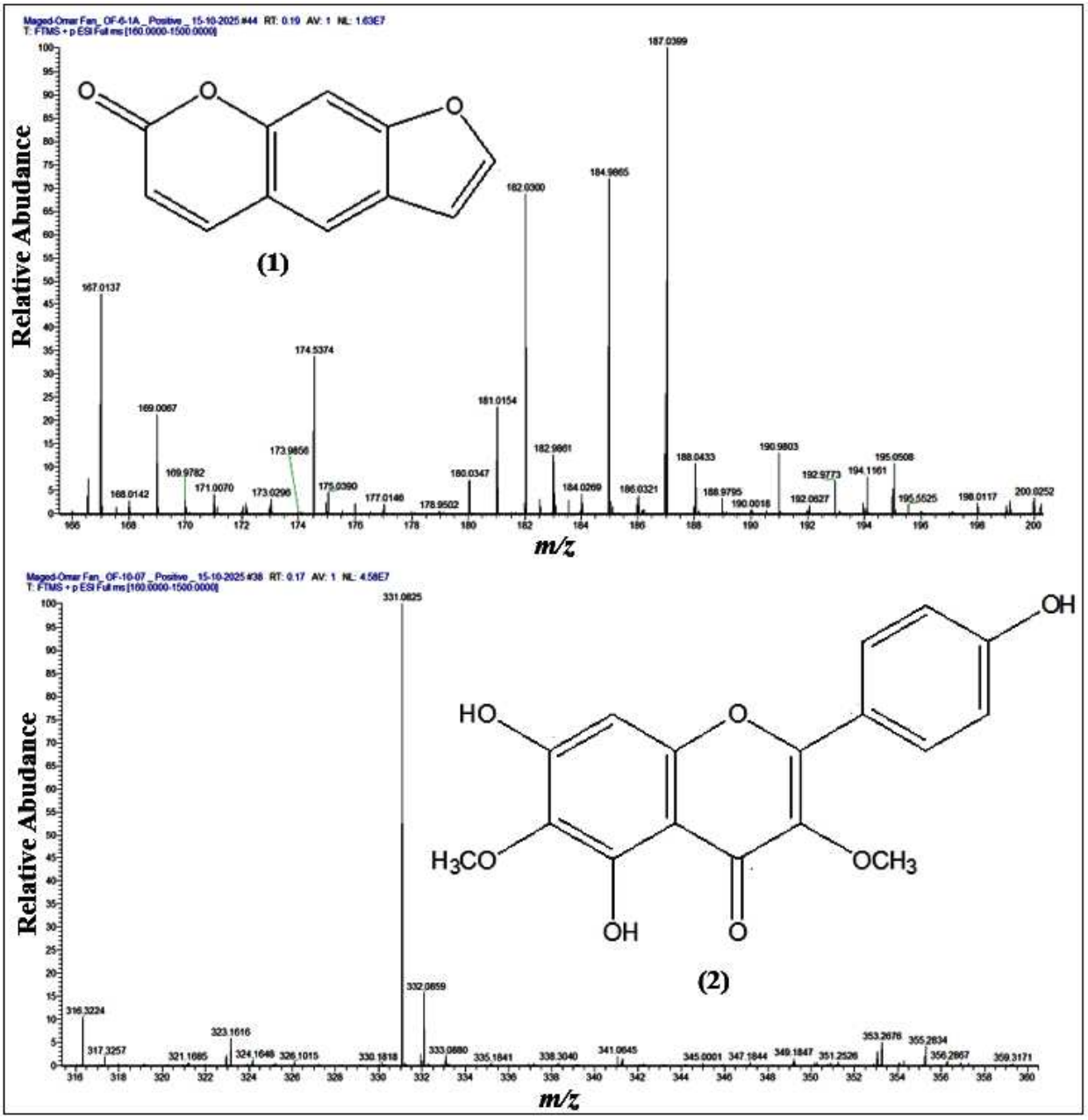


Fig. 1 Chemical structure of compounds (1,2) isolated from aerial parts of *O. fruticosa*

Antibacterial activity of psoralen and galetin 3,6-dimethyl ether against P. aeruginosa

The antibacterial activity of psoralen (compound **1**) and galetin 3,6-dimethyl ether (compound **2**) against the opportunistic Gram-negative pathogen *P. aeruginosa* was evaluated by determining their MIC and percentage growth inhibition. Both phytochemicals demonstrated remarkable efficacy in suppressing bacterial proliferation, underscoring their potential as viable alternative

antimicrobial agents to combat rising antibiotic resistance (Table 1). Among the tested compounds, Galetin 3,6-dimethyl ether exhibited superior primary antibacterial efficacy, characterized by a lower MIC of 125 μg/mL and a high growth inhibition rate of 96.83%. This lower MIC indicates higher baseline affinity and intracellular penetration capacity, allowing the flavonoid structure to effectively arrest bacterial replication at reduced dosages. In contrast, psoralen demonstrates an MIC of 175 μg/mL alongside an exceptionally high growth inhibition of 98.93%, indicating substantial suppression of bacterial proliferation despite requiring a slightly higher threshold concentration. The profound growth inhibition displayed by both phytochemicals points toward multifaceted, multi-target mechanisms of action against *P. aeruginosa*. At the cellular level, the lipophilic regions of both the furocoumarin and methylated flavonol skeletons enable direct interaction with the bacterial phospholipid bilayer, compromising membrane integrity, increasing permeability, and precipitating the leakage of vital intracellular metabolites.

Table 1 Minimum inhibitory concentration (MIC) and growth inhibition of psoralen and Galetin 3,6-dimethyl ether against *P. aeruginosa*.

Bacterial strain	Compound name	MIC (μg/mL)	Percentage Inhibition (%)
P. aeruginosa	Psoralen	175	98.93
P. aeruginosa	Galetin 3,6-dimethyl ether	125	96.83

Assessment of Membrane Integrity

The impact of psoralen and galetin 3,6-dimethyl ether on *P. aeruginosa* membrane integrity was evaluated by measuring extracellular leakage of intracellular macromolecules, specifically proteins and nucleic acids. Treatment with both compounds resulted in a statistically significant increase in extracellular protein leakage compared to the untreated control (3.75 ± 0.27 mg/mL). Exposure to psoralen induced a pronounced increase in protein concentration to 5.56 ± 0.21 mg/mL (43% increase), whereas galetin 3,6-dimethyl ether elevated protein levels to 4.30 ± 0.64 mg/mL (14.7% increase; one-way ANOVA, $F(2,6) = 35.38$, $p < 0.001$) (Fig. 2a). In alignment with these

findings, extracellular nucleic acid levels also rose significantly from 198.93 ± 8.32 ng/mL in the control to 308.23 ± 9.67 ng/mL with psoralen and 256.73 ± 24.45 ng/mL with galetin 3,6-dimethyl ether, representing increases of approximately 54.9% and 29.1%, respectively (Fig. 2b). One-way ANOVA indicated significant differences among the treatment groups for both protein and nucleic acid leakage (F (2,6) = 35.38, $p < 0.001$).

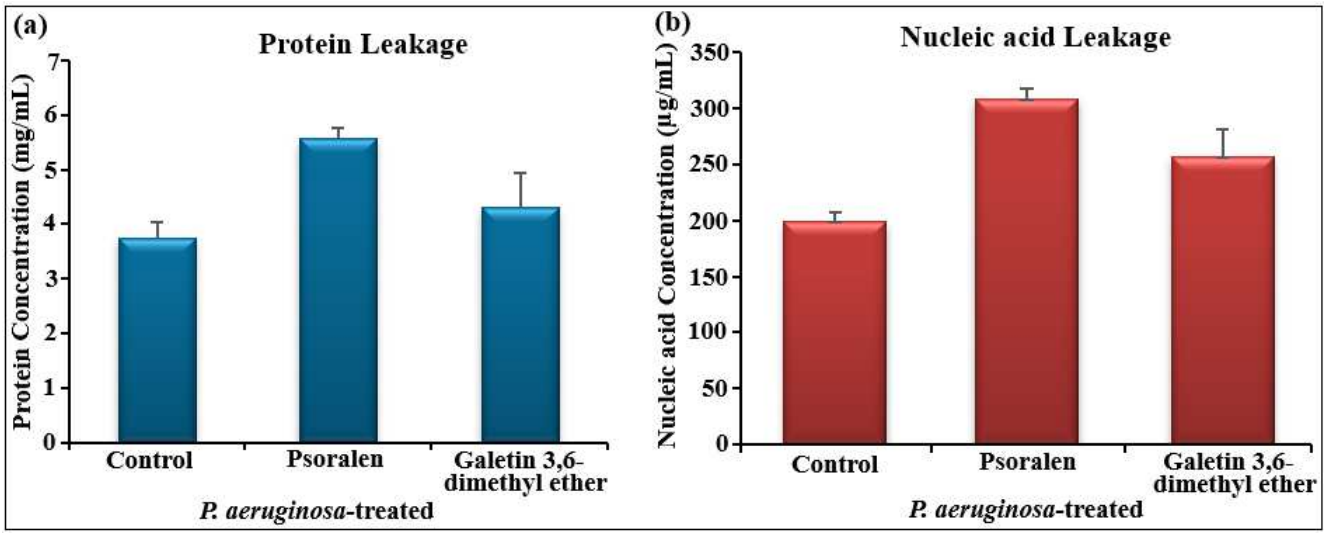


Fig. 2 Leakage of (a) proteins and (b) nucleic acids from Pseudomonas aeruginosa following treatment with psoralen and galetin 3,6-dimethyl ether, compared with the untreated control. Psoralen induced significantly greater protein leakage than galetin 3,6-dimethyl ether and the control. Data are expressed as mean ± SD (n = 3); $**p < 0.001$, as determined by one-way ANOVA followed by Tukey's post hoc test.

Across both assays, psoralen consistently demonstrated a markedly stronger capacity to induce macromolecular leakage compared to galetin 3,6-dimethyl ether. This differential response suggests distinct molecular interactions with the lipid bilayer, where psoralen's chemical structure may promote more severe membrane defects, such as pore formation or bilayer destabilization[37]. Overall, these combined leakage assays confirm that membrane permeabilization and cell-envelope structural damage constitute a major mechanism underlying the antimicrobial activity of both phytochemicals, particularly psoralen[38, 39]. The concurrent release of proteins and nucleic

acids strongly indicates substantial perturbation of the cell envelope and an increase in cytoplasmic membrane permeability. Intact bacterial membranes serve as selective barriers that strictly restrict the extracellular efflux of large macromolecules, such as DNA, RNA, and structural or enzymatic proteins[40]. Irreversible cell-envelope disruption facilitates the rapid loss of these critical cytoplasmic components, which subsequently destabilizes essential physiological processes including ion homeostasis, nutrient transport, transmembrane potential maintenance, and energy metabolism, ultimately leading to cell death[41, 42]. These findings indicate that both psoralen and Galetin 3,6-dimethyl ether possess promising anti-*P. aeruginosa* properties and may serve as potential candidates for further mechanistic, antibiofilm, and molecular docking investigations targeting virulence-associated pathways in *P. aeruginosa*

Anti-biofilm and anti-quorum sensing activities

Anti-biofilm activity was evaluated using confocal laser scanning microscopy (CLSM), which revealed pronounced alterations in *P. aeruginosa* biofilm architecture after treatment with psoralen and galetin 3,6-dimethyl ether (Fig. 3, Table 2). The untreated control exhibited a dense, compact, and well-developed biofilm with extensive surface coverage, consistent with the characteristic three-dimensional organization of *P. aeruginosa* biofilms described previously [43]. Quantitatively, the control biofilm demonstrated mean red and green fluorescence intensities of 47.50 ± 11.85 and 40.88 ± 0.67, respectively, alongside a mean biofilm thickness of 98.00 ± 2.00 μm. Treatment with psoralen (175 μg/mL) markedly disrupted the biofilm structure and reduced biofilm-associated fluorescence. Red fluorescence decreased to 7.56 ± 0.34, corresponding to an 84.1% reduction, whereas green fluorescence declined to 3.11 ± 0.66, representing a 92.4% reduction relative to the untreated control. Mean biofilm thickness also decreased to 83.00 ± 15.39 μm, representing an approximate 15.3% reduction. Similarly, galetin 3,6-dimethyl ether (125 μg/mL) induced

substantial structural breakdown, reducing red fluorescence to 3.96 ± 2.89 (a 91.7% decrease) and green fluorescence to 7.18 ± 6.11(an 82.4% decrease), with a mean biofilm thickness of 88.67 ± 23.01 μm (~9.5% reduction) (Table 2).

Table 2 Effects of psoralen and galetin 3,6-dimethyl ether on red and green fluorescence intensities, biofilm thickness, and red fluorescence reduction in *P. aeruginosa* biofilms.

Compound/Control	Dosage (μg/mL)	Red Fluorescence Intensity (Mean ± SD)	Green Fluorescence Intensity (Mean ± SD)	Mean Biofilm Thickness (μm) (Mean ± SD)	Reduction in Red Fluorescence (%)	Reduction in Red Fluorescence (%)
P.aeruginosa	0.0	47.50 ± 11.85	40.88 ± 0.67	98.00 ± 2.00	-	-
Psoralen	175	7.56 ± 0.34	3.11 ± 0.66	83.00 ± 15.39	84.1	92.4
Galetin 3,6-dimethyl ether	125	3.96 ± 2.89	7.18 ± 6.11	88.67 ± 23.01	91.7	82.4

[CLSM images of P. aeruginosa biofilms treated with psoralen (175 μg/mL) or galetin 3,6-dimethyl ether (125 μg/mL), compared with the untreated control. Live and dead cells appear green and red, respectively. Fluorescence intensity, biofilm thickness, and percentage reductions are expressed as mean ± SD.]

Microscopic evaluation confirmed a more dispersed biofilm architecture with significantly reduced cellular density compared with the compact control (Fig. 3a), reflecting impaired organizational stability and extracellular matrix integrity[44]. The simultaneous decline in both SYTO 9-associated green fluorescence (intact cells) and propidium iodide–associated red fluorescence (membrane-compromised cells) indicates an overall reduction in total biofilm-associated biomass rather than localized cell killing alone[45]. Because structural disruption and detachment lower the absolute abundance of both viable and non-viable populations, the decreased red fluorescence should not be interpreted independently as reduced antimicrobial activity, but rather as evidence of comprehensive biomass removal. Notably, psoralen produced a greater reduction in green fluorescence (92.4%) and a larger numerical decrease in thickness (Fig. 3b), whereas galetin 3,6-dimethyl ether caused the highest reduction in red fluorescence (91.7%, Fig. 3c). However, given the high variability in thickness observed in treated groups, particularly with galetin 3,6-dimethyl ether, formal statistical testing is required before asserting significant differences in structural thickness.

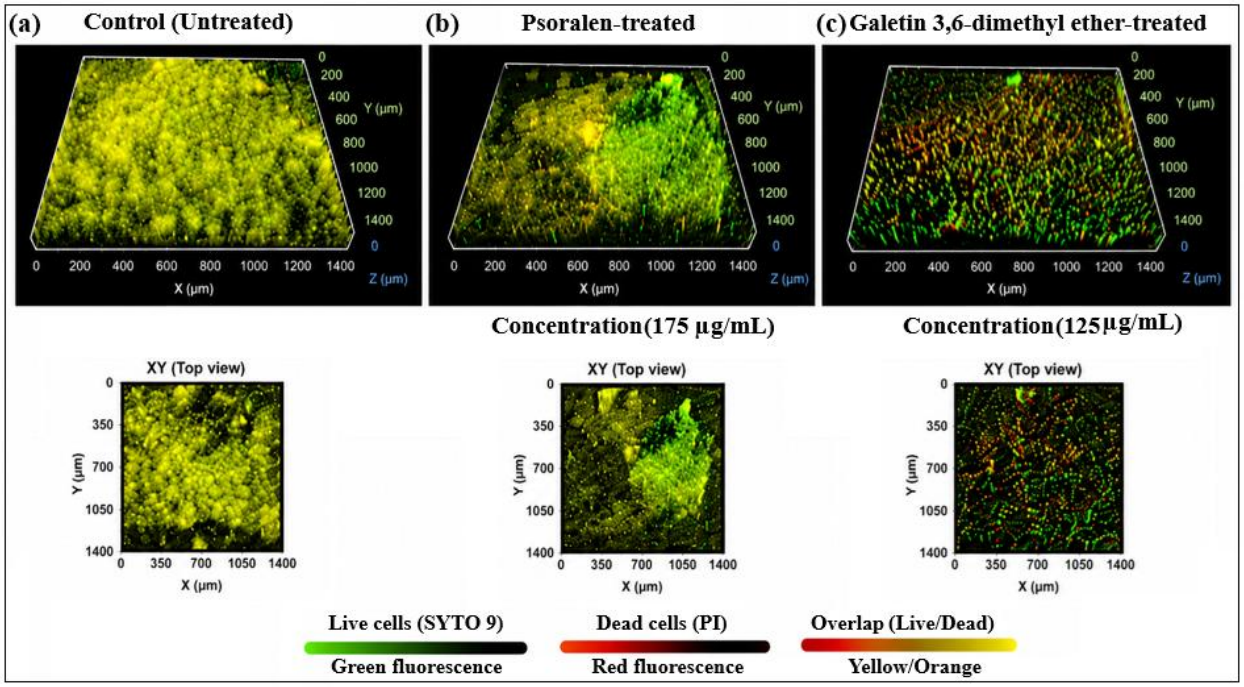


Fig. 3 Confocal laser scanning microscopy (CLSM) images of *P. aeruginosa* biofilms: (a) untreated control, (b) psoralen-treated biofilm, and (c) biofilm treated with galetin 3,6-dimethyl ether.

These substantial structural breakdowns and biomass reductions are tightly linked to the disruption of bacterial cell-to-cell communication networks. Quorum sensing, alongside extracellular polymeric substance (EPS) production, flagellar/pili motility, and intercellular coordination, serves as a master regulator governing *P. aeruginosa* biofilm maturation, structural persistence, and virulence[46]. Disrupting quorum sensing compromises the bacterial signaling needed for coordinated cellular aggregation, making the biofilm architecture fragile, dispersed, and increasingly susceptible to clearance. In particular, the marked antibiofilm efficacy and structural collapse induced by psoralen align with its established role as a potent quorum-sensing inhibitor that attenuates *P. aeruginosa* virulence and interferes with quorum-regulated developmental processes[47]. By interfering with these regulatory signaling cascades, psoralen and galetin 3,6-

dimethyl ether weaken the structural stability of the biofilm matrix, preventing the establishment of dense, mature bacterial communities.

Structure–activity relationships of psoralen and galetin 3,6-dimethyl ether in antibacterial and antibiofilm activity

The antibacterial and antibiofilm properties of psoralen and galetin 3,6-dimethyl ether stem from their distinct aromatic scaffolds and oxygen-containing functional groups, which facilitate critical noncovalent interactions with the cell envelope of *P. aeruginosa*. As a Gram-negative pathogen, *P. aeruginosa* relies on an outer permeability barrier rich in lipopolysaccharides (LPS), phospholipids, and membrane proteins[3]. The structural features of these phytochemicals enable them to engage in this complex architecture through hydrophobic association and hydrogen bonding, potentially disturbing envelope organization and barrier function. Psoralen, a planar furocoumarin, possesses a fused tricyclic aromatic system featuring a conjugated lactone carbonyl and ether oxygen atoms. Its rigid, conjugated geometry and hydrophobic surface favor partitioning into lipid-rich domains of the bacterial envelope. This partitioning perturbs local lipid packing, increases membrane permeability, and promotes the leakage of intracellular constituents[20]. Although its carbonyl and ether groups can participate in dipolar interactions with polar membrane constituents, psoralen lacks a strongly ionizable group under physiological conditions. Consequently, its affinity for the negatively charged LPS layer cannot be deduced from structure alone, meaning its overall membrane effects rely heavily on molecular orientation and environmental composition. In contrast, galetin 3,6-dimethyl ether features an aromatic flavonoid scaffold containing a carbonyl group, ether linkages derived from the methylation of the 3- and 6-hydroxyl positions, and remaining phenolic hydroxyl functionalities. Its aromatic framework drives hydrophobic interactions with membrane lipids, while the carbonyl and hydroxyl groups

form hydrogen bonds with polar headgroups and envelope proteins. Methylation modifies the molecule's hydrogen-bond-donating capacity, polarity, and lipophilicity by reducing free hydroxyl groups[48]. Although these alterations influence partitioning and cellular uptake, the net impact on antibacterial potency depends on molecular conformation and aqueous solubility.

These structural differences align with their experimental profiles: galetin 3,6-dimethyl ether showed a lower MIC of 125 μg/mL compared to 175 μg/mL for psoralen, indicating higher overall potency. However, psoralen induced greater extracellular protein leakage, highlighting that the magnitude of protein release did not directly correlate with MIC values. This divergence underscores differences in membrane interaction dynamics, cellular uptake, or intracellular targets rather than direct correlations with potency. Beyond bactericidal action, both metabolites exhibit robust antibiofilm potential. They inhibit initial cell adhesion by altering surface charge distribution and outer membrane protein conformation. Furthermore, they may disrupt quorum-sensing networks that coordinate extracellular polymeric substance (EPS) production and biofilm architecture. Finally, their low molecular weights and moderate lipophilicity allow them to penetrate mature biofilms, destabilizing persister cell membranes and diminishing overall community viability. The proposed mechanisms are schematically illustrated in Figs. 4a and 4b, highlighting the potential contributions of molecular structure to membrane interactions, bacterial damage, and biofilm inhibition.

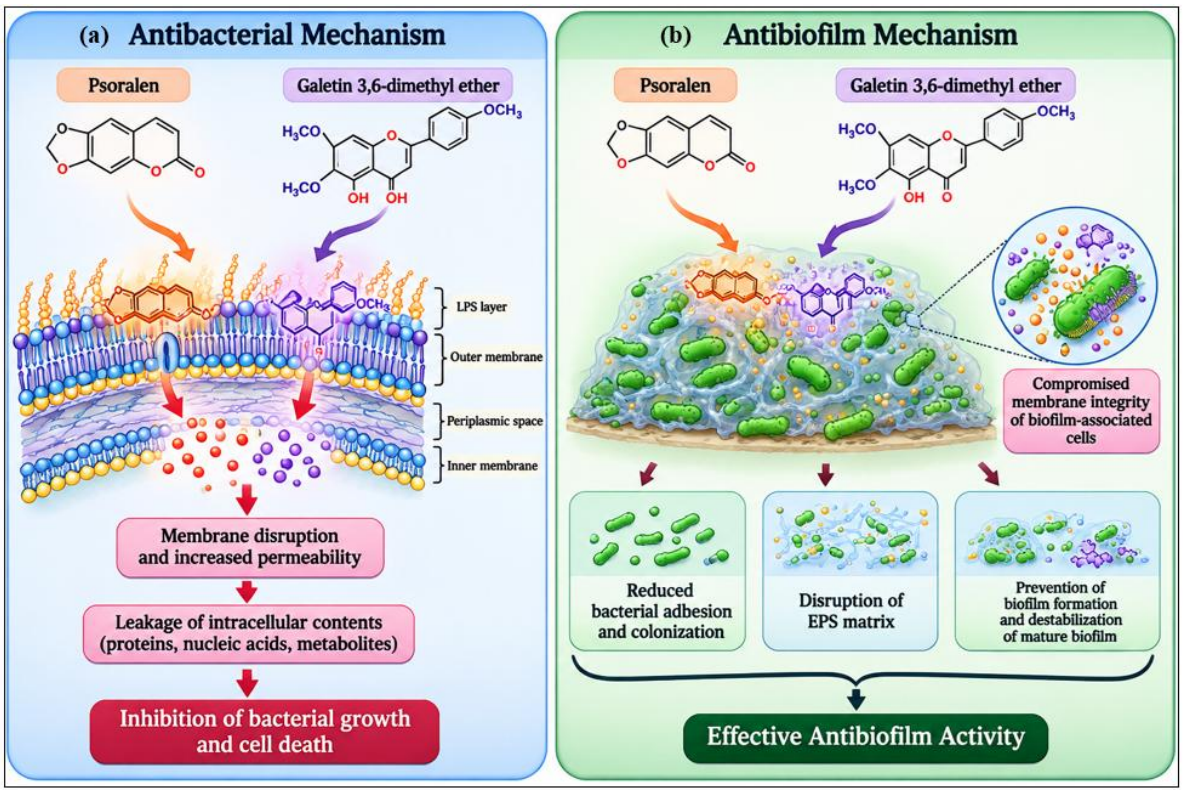


Fig. 4 Proposed mechanism of (a) antibacterial and (b) anti-biofilm activity of psoralen and galetin 3,6-dimethyl ether isolated from aerial parts of *O. fruticosa*

Molecular docking analysis of psoralen and galetin 3,6-dimethyl ether

To gain further insight into the potential molecular interactions underlying the antibacterial and antibiofilm activities of these compounds, molecular docking analysis was performed to investigate the binding interactions of psoralen and galetin 3,6-dimethyl ether with the key quorum-sensing regulatory proteins LasR and RhlR of *P. aeruginosa*, respectively. Azithromycin was used as a reference ligand for comparative evaluation of the predicted binding affinities and interaction profiles. Psoralen exhibited a docking score of −7.47 kcal/mol against LasR, compared with −20.16 kcal/mol for azithromycin. Similarly, galetin 3,6-dimethyl ether yielded a docking score of −6.94 kcal/mol against RhlR, whereas azithromycin scored −9.92 kcal/mol (Tables 3 and 4). These negative docking scores indicate that both phytochemicals fit favorably into the active

sites of their respective receptors, though their predicted binding scores were less negative than those of the reference ligand.

Table 3 Molecular docking interaction profiles of psoralen, galetin 3,6-dimethyl ether, and azithromycin against LasR and RhlR of *P. aeruginosa*

Protein(receptor) and Ligand	Binding energy (kcal/mol)	No. of H bonds	Amino acids involved in H-bond interaction	Hydrophobic Interactions	Amino acids involved in Hydrophobic interactions	Electrostatic interaction	Amino acids involved in Electrostatic interaction
Pseudomonas aeruginosa **LasR** and **Psoralen**	-7.47	3	TRP60 ;TYR64	NA	NA	NA	NA
Pseudomonas aeruginosa ***LasR*** *and* **Azithromycin**	-20.16	2	TRP60 ;LEU125	4	TYR56,60,64 ;ILE52	8	ASP65,73 ;TYR64 ;GLU48
Pseudomonas aeruginosa **RhlR** and **Galetin 3,6-dimethyl ether**	-6.94	5	GLU182 ;HIS71,159, 221 ;ASP178	NA	NA	NA	NA
Pseudomonas aeruginosa **RhlR** and **Azithromycin**	-9.92	7	HIS71 ;ARG288 ;SER285 ;ALA105 ;PHE195 ;TYR72 ;ASP73	NA	NA	4	HIS71 ;PHE195

[Molecular docking analysis comparing **psoralen, galetin 3,6-dimethyl ether** and **azithromycin** interactions with LasR and RhlR protein from *P. aeruginosa*]

Analysis of the predicted binding poses provided further insights into the potential molecular interactions underlying ligand recognition. Psoralen was stably accommodated within the active pocket of LasR, forming hydrogen bonds with key residues Trp60 and Tyr64 (Fig. 5). These specific residues frequently participate in stabilizing planar or aromatic ligands within the core of the LasR binding cavity, facilitating proper spatial orientation and hydrophobic packing.

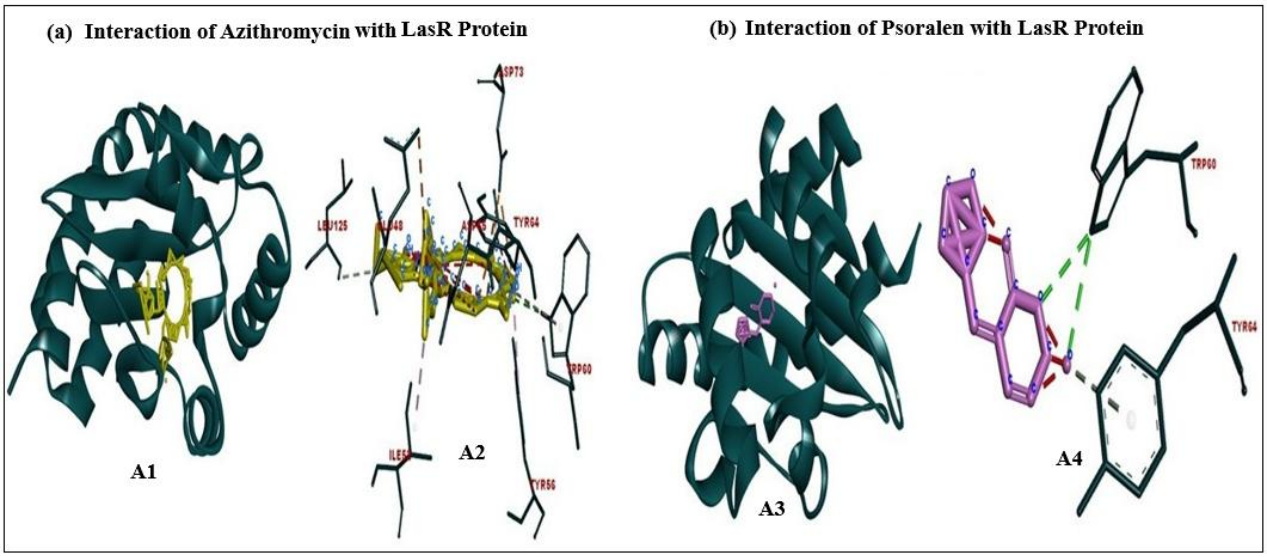


Figure 5. Molecular docking analysis of (a) azithromycin and (b) psoralen with the LasR quorum-sensing regulator of *P aeruginosa*. Docking poses and interaction profiles of azithromycin and psoralen with the LasR protein of *P. aeruginosa*. Panels A1–A4 illustrate the three-dimensional binding conformations and residue-level interactions within the LasR binding pocket.

Meanwhile, galetin 3,6-dimethyl ether established a complex network of hydrogen bonds with Glu182, His71, His159, His221, and Asp178 within the RhlR binding domain (Fig. 6). The involvement of multiple histidine and polar acidic residues highlights a multi-point anchoring mechanism that contributes significantly to electrostatic stabilization, charge distribution, and polar complementarity within the RhlR active site. Nevertheless, the significance of individual residues depends on their spatial arrangement, interaction geometry, and the physicochemical environment of the binding site. Thus, the predicted interactions identify plausible molecular contact points but do not independently confirm receptor binding or establish the functional importance of the interacting residues.

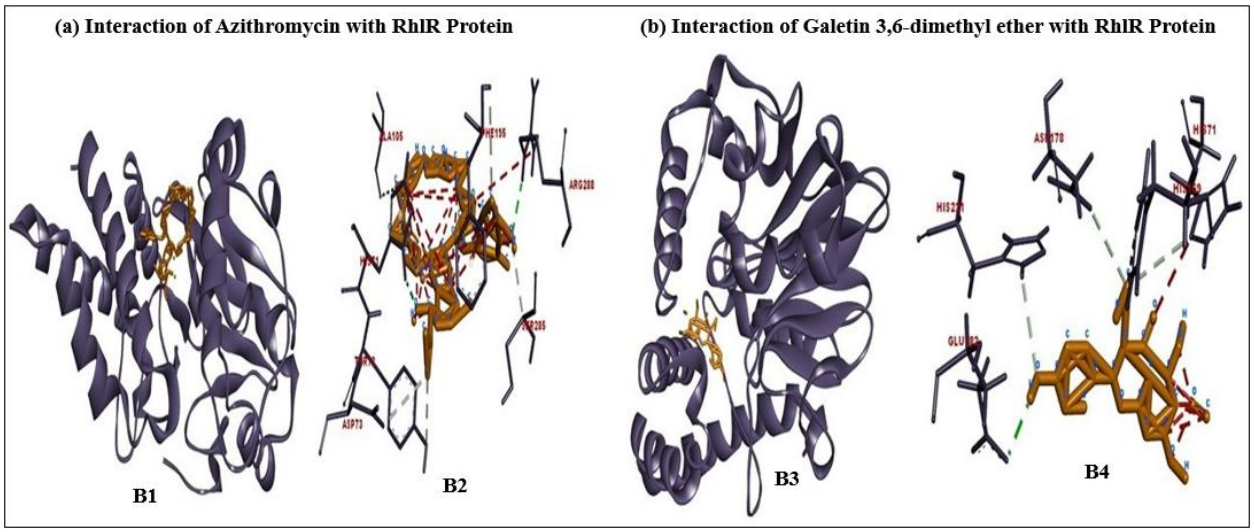


Fig. 6 Molecular docking analysis of (a) azithromycin and (b) Galetin 3,6-dimethyl ether with the RhlR quorum-sensing regulator of *P. aeruginosa*. Docking poses and interaction profiles of azithromycin and galetin 3,6-dimethyl ether with the RhlR quorum-sensing regulator of Pseudomonas aeruginosa. Panels B1–B4 illustrate the three-dimensional binding conformations and key molecular interactions within the RhlR ligand-binding pocket.

These computational predictions provide a plausible structural foundation for the observed antibiofilm and anti-quorum sensing activities. In *P. aeruginosa,* LasR and RhlR are master transcriptional regulators governing virulence factor expression, extracellular matrix synthesis, motility, and biofilm maturation[49, 50]. Competitive binding or steric obstruction of these active sites by psoralen and galetin 3,6-dimethyl ether offers a mechanistic rationale for the disrupted biofilm architecture and reduced biomass observed experimentally. The predicted interaction of psoralen with LasR is of particular interest because this regulatory protein plays a central role in coordinating quorum-sensing-dependent virulence responses, while RhlR similarly regulates several virulence-associated phenotypes and bacterial social behaviors. Interference with these regulatory pathways could potentially alter virulence-factor expression and contribute to changes in biofilm development, aligning with the observed architectural disruption following treatment with psoralen and galetin 3,6-dimethyl ether.

However, mathematical conversions of docking score differences ($\Delta\Delta G$ of −12.69 kcal/mol for the LasR and −2.98 kcal/mol for the RhlR) into theoretical binding fold-changes (such as 2.4×10^9 for LasR or 153.51 for RhlR) are non-rigorous and should not be presented as true thermodynamic affinity ratios (Table 4). Direct translation of empirical docking scores into kinetic constants requires free-energy perturbation (FEP) methods or empirical biophysical measurements.

Table 4 Comparison of relative binding affinity of psoralen, galetin 3,6-dimethyl ether and azithromycin interactions with LasR and RhlR protein from *P. aeruginosa*

Receptor	ΔG Psoralen (kcal/mol)	ΔG Azithromycin (kcal/mol)	ΔΔG (kcal/mol)	Fold Difference (Kd ratio)	Interpretation
P. aeruginosa **LasR**	-7.47	-20.16	-12.69	2.04×10^9	Psoralen demonstrated favorable binding toward the LasR receptor; however, azithromycin exhibited substantially stronger thermodynamic stability and binding affinity under the same docking conditions.
Receptor	**ΔG Galetin 3,6-dimethyl ether (kcal/mol)**	**ΔG Azithromycin (kcal/mol)**	**ΔΔG (kcal/mol)**	**Fold Difference (Kd ratio)**	**Interpretation**
P. aeruginosa **RhlR**	-6.94	-9.92	-2.98	153.51	Galetin showed moderate and stable interaction with the RhlR receptor, although azithromycin displayed comparatively stronger binding affinity and receptor stabilization.

Thus, molecular docking identified plausible interactions of psoralen with LasR and galetin 3,6-dimethyl ether with RhlR, providing a basis for further investigation of their potential involvement in QS-associated antibiofilm activity. Although the predicted binding poses and hydrogen-bonding patterns offer mechanistic hypotheses consistent with the observed disruption of biofilm architecture, functional inhibition of these regulatory proteins remains unconfirmed. Further validation using LasR- and RhlR-responsive reporter assays, assessment of QS-regulated virulence factors, and, where feasible, direct binding studies would help establish whether these compounds interfere with QS signaling. Appropriate bacterial growth and viability controls would also be essential to distinguish specific QS-related effects from indirect consequences of antimicrobial activity.

Conclusion

This study establishes the isolation of two phenolic phytoconstituents, psoralen and galetin 3,6-dimethyl ether, from the methanolic extract of O. fruticosa for the first time, with their chemical structures elucidated via spectroscopic characterization. This significantly expands the chemotaxonomic profile of the genus *Otostegia*. Both isolated phytochemicals demonstrated

substantial antibacterial and antibiofilm activities against *P. aeruginosa*. Galetin 3,6-dimethyl ether exhibited greater antibacterial potency based on its lower MIC of 125 µg/mL, whereas psoralen produced a slightly higher percentage of metabolic growth inhibition. Confocal microscopy showed that both compounds markedly reduced biofilm-associated fluorescence, cellular density, and three-dimensional structural organization. Psoralen produced the greatest reduction in membrane-intact-cell-associated green fluorescence and mean biofilm thickness, whereas Galetin 3,6-dimethyl ether caused the strongest reduction in PI-associated red fluorescence. The simultaneous depletion of green and red fluorescence indicates an overall reduction or detachment of biofilm-associated cellular material rather than merely a shift from membrane-intact to membrane-compromised populations. Molecular docking predicted favorable interactions of psoralen with LasR and Galetin 3,6-dimethyl ether with RhlR, suggesting that interference with quorum-sensing regulation may contribute to their antibiofilm effects. However, these predicted mechanisms require experimental confirmation. Overall, the findings identify psoralen and Galetin 3,6-dimethyl ether as promising natural lead compounds for the development of alternative or adjunctive strategies against persistent *P. aeruginosa* infections. Further investigations incorporating bactericidal assays, biofilm viable counts, quorum-sensing reporter systems, virulence-factor quantification, gene-expression analysis, cytotoxicity assessment, and *in vivo* infection models are warranted.

Author contributions

GAA: Conceptualization, Visualization, Supervision. BMM: Formal Analysis, Data Curation. AM: Data Curation, Visualization, Project administration, Writing – Original Draft. MA: Investigation, Methodology, Data Curation, Resources, Validation, Writing – Original Draft, Writing – Review & Editing. All authors reviewed and approved the final manuscript.

Funding

This research project was supported by Ongoing Research Funding Program, (ORF-2026-1654), King Saud University, Riyadh, Saudi Arabia.

Data Availability Statement

All data generated or analyzed during this study are included in this article.

Declarations

Competing interests

The authors declare no competing interests.

References

1. Karnwal, A., Jassim, A. Y., Mohammed, A. A., Al-Tawaha, A. R., Selvaraj, M. & Malik, T. Addressing the global challenge of bacterial drug resistance: insights, strategies, and future directions. *Front. Microbiol.* **16**, 1517772 (2025). https://doi.org/10.3389/fmicb.2025.1517772
2. Pache, M., Nikam, S. & Jagtap, M. Antibiotic resistance: current challenges and future directions. *Int. J. Pharm. Sci.* **3**, 1600–1622 (2025). https://www.ijpsjournal.com/
3. Alharbi, M. S. et al. Multidrug-resistant *Pseudomonas aeruginosa*: pathogenesis, resistance mechanisms, and novel therapeutic strategies. *Virulence* **16**, 2580160 (2025). https://doi.org/10.1080/21505594.2025.2580160
4. Elfadadny, A. et al. Antimicrobial resistance of *Pseudomonas aeruginosa*: navigating clinical impacts, current resistance trends, and innovations in breaking therapies. *Front. Microbiol.* **15**, 1374466 (2024). https://doi.org/10.3389/fmicb.2024.1374466

5. Zhao, Y., Xu, H., Wang, H., Wang, P. & Chen, S. Multidrug resistance in *Pseudomonas aeruginosa*: genetic control mechanisms and therapeutic advances. *Mol. Biomed.* **5**, 62 (2024). https://doi.org/10.1186/s43556-024-00221-y
6. Reynolds, D. & Kollef, M. The epidemiology, pathogenesis, and treatment of *Pseudomonas aeruginosa* infections: an update. *Drugs* **81**, 2117–2131 (2021). https://doi.org/10.2165/00003495-200767030-00003
7. Zhang, X., Zhang, D., Zhou, D., Zheng, S., Li, S., Hou, Q., Li, G. & Han, H. A comprehensive review of the pathogenic mechanisms of *Pseudomonas aeruginosa*: synergistic effects of virulence factors, quorum sensing, and biofilm formation. *Front. Microbiol.* **16**, 1619626 (2025). https://doi.org/10.3389/fmicb.2025.1619626
8. Borisova, D., Paunova-Krasteva, T., Strateva, T. & Stoitsova, S. Biofilm formation of *Pseudomonas aeruginosa* in cystic fibrosis: mechanisms of persistence, adaptation, and pathogenesis. *Microorganisms* **13**, 1527 (2025). https://doi.org/10.3390/microorganisms13071527
9. Ramzan, S., Kanwal, M. & Hassan, M. A. Microbial biofilms and their molecular mechanisms in pathogenesis, antimicrobial resistance, and infection persistence. *Res. Consortium Arch.* **4**, 4883–4896 (2026). https://doi.org/10.5281/zenodo.22991525
10. Zou, W., Lin, R., Zhao, Y., Zhan, P., Zhao, X. & Zhang, Q. Biofilm-mediated antibiotic tolerance in bacterial pathogens: integrated molecular networks and novel therapeutic avenues. *Virulence* **17**, 2687214 (2026). https://doi.org/10.1080/21505594.2026.2687214
11. Qureshi, K. A., Fahmy, N. A., Parvez, A., Almahasheer, H., Permatasari, D., Jaremko, M. & Abdallah, E. M. Biofilms and antimicrobial resistance: mechanisms, clinical

implications, and emerging interventions. *Chem. Biodivers.* **23**, e01351 (2026). https://doi.org/10.1002/cbdv.202501351

12. Supardy, N. A. & Kumar, R. R. Aging, biofilms, and diabetic foot ulcers: disrupting chronic infections with super-oxidized solutions and addressing age-related vulnerabilities. *Cardiovasc. Diabetol. Endocrinol. Rep.* **11**, 45 (2025). https://doi.org/10.1186/s40842-025-00261-5
13. Ruga, S. et al. Plant-derived compounds as antibiotic adjuvants against drug-resistant ESKAPE pathogens: mechanisms of action, synergistic strategies, and translational challenges. *Antibiotics* **15**, 761 (2026). https://doi.org/10.3390/antibiotics15080761
14. Hawwal, M. F., Ahmed, S., Alam, P., Fantoukh, O. I., AlHamoud, G. A., Alharbi, H. A., Alobaid, W. A. & Khojah, H. *Otostegia fruticosa* (Forssk.)—a comprehensive insight of its ethnopharmacology, phytochemistry, and pharmacological activities. *Saudi Pharm. J.* **32**, 102189 (2024). https://doi.org/10.1016/j.jsps.2024.102189
15. Bahta, T., Karim, A., Periasamy, G., Gebremedhin, G., Bitew, H. & Hagazi, K. Analgesic, anti-inflammatory and in vitro hyaluronidase inhibitory properties of the leaf extract and solvent fractions of *Otostegia fruticosa* (Forssk.) Schweinf. ex Penzig. *Iran. J. Pharm. Res.* **19**, 218 (2020). https://doi.org/10.22037/ijpr.2019.14657.12569
16. Ansari, M. N., Rehman, N. U., Karim, A., Bahta, T., Abujheisha, K. Y., Ahamad, S. R. & Imam, F. Evaluation of bronchodilatory and antimicrobial activities of *Otostegia fruticosa*: a multi-mechanistic approach. *Saudi Pharm. J.* **28**, 281–289 (2020). https://doi.org/10.1016/j.jsps.2020.01.007
17. Ali, N. A., Alhamzy, E. H., Chhetri, B. K., Dosoky, N. S. & Setzer, W. N. Chemical composition, antimicrobial, and cytotoxic activities of the essential oil of *Otostegia*

fruticosa subsp. *schimperi* from Yemen. *Nat. Prod. Commun.* **12**, 1934578X1701200634 (2017). https://doi.org/10.1177/1934578X1701200634

18. Hu, Y. Y., Wang, Y. C., Qin, W. X., Yu, S., Dai, S. Y., Pei, Y. H., Li, C. & Yang, Y. H. Pharmaceutical design and structure–activity relationships of psoralen and derivatives. *Curr. Pharm. Des.* **31**, 2438–2463 (2025). https://doi.org/10.2174/0113816128365838250128060007
19. Tripathi, N., Bhardwaj, N., Kumar, S. & Jain, S. K. Phytochemical and pharmacological aspects of psoralen—a bioactive furanocoumarin from *Psoralea corylifolia* Linn. *Chem. Biodivers.* **20**, e202300867 (2023). https://doi.org/10.1002/cbdv.202300867
20. Galiatsatos, P. et al. Psoralen: a narrative review of current and future therapeutic uses. *J. Cancer Res. Clin. Oncol.* **150**, 130 (2024). https://doi.org/10.1007/s00432-024-05648-y
21. Devi, C. S. Anti-inflammatory and analgesic actions of 4′,5,6-trihydroxy-3′,7-dimethoxyflavone from *Vicoa indica* DC. *Indian J. Pharmacol.* **29**, 178–181 (1997).
22. Macêdo, C. L., Vasconcelos, L. H., Correia, A. C., Martins, I. R., de Lira, D. P., de Oliveira Santos, B. V. & da Silva, B. A. Spasmolytic effect of galetin 3,6-dimethyl ether, a flavonoid obtained from *Piptadenia stipulacea* (Benth.) Ducke. *J. Smooth Muscle Res.* **47**, 123–134 (2011). https://doi.org/10.1540/jsmr.47.123
23. Carreiro, J. D., Souza, I. L., Pereira, J. C., Vasconcelos, L. H., Travassos, R. D., Santos, B. V. & Silva, B. A. Tocolytic action and underlying mechanism of galetin 3,6-dimethyl ether on rat uterus. *BMC Complement. Altern. Med.* **17**, 514 (2017). https://doi.org/10.1186/s12906-017-2007-6

24. Rashid, A., Khan, A. A., Dar, S. H., Ahmad, Y., Nabi, N. G., Ganaie, M. A. & Teli, A. R. Extraction, isolation and spectral analysis of the psoralen compound from *Ficus carica* Linn. leaves. *Pharma Innov. J.* **6**, 740–743 (2017).

25. Van Heerden, F. R., Viljoen, A. M. & Van Wyk, B. E. The major flavonoid of *Dodonaea angustifolia*. *Fitoterapia* **71**, 602–604 (2000). https://doi.org/10.1016/S0367-326X(00)00201-X

26. Lu, H., Zhang, L., Liu, D., Tang, P. & Song, F. Isolation and purification of psoralen and isopsoralen and their efficacy and safety in the treatment of osteosarcoma in nude rats. *Afr. Health Sci.* **14**, 641 (2014). https://doi.org/10.4314/ahs.v14i3.20

27. Hulankova, R. Methods for determination of antimicrobial activity of essential oils in vitro—a review. *Plants* **13**, 2784 (2024). https://doi.org/10.3390/plants13192784

28. Nguyen, T. P., Van Duong, T., Le, T. Q. & Nguyen, K. T. Uncovering the antibacterial potential of a peptide-rich extract of edible bird's nest against *Staphylococcus aureus*. *J. Microbiol. Biotechnol.* **34**, 1680 (2024). https://doi.org/10.4014/jmb.2402.02052

29. Pezzoni, M., Pizarro, R. A. & Costa, C. S. Evaluation of viable cells in *Pseudomonas aeruginosa* biofilms by colony count and live/dead staining. *Bio-protocol* **10**, e3762 (2020). https://doi.org/10.21769/BioProtoc.3762

30. Stiefel, P., Schmidt-Emrich, S., Maniura-Weber, K. & Ren, Q. Critical aspects of using bacterial cell viability assays with the fluorophores SYTO9 and propidium iodide. *BMC Microbiol.* **15**, 36 (2015). https://doi.org/10.1186/s12866-015-0376-x

31. RCSB Protein Data Bank. RCSB PDB: homepage. https://www.rcsb.org/ (accessed 14 May 2026).

32. O'Boyle, N. M., Banck, M., James, C. A., Morley, C., Vandermeersch, T. & Hutchison, G. R. Open Babel: an open chemical toolbox. *J. Cheminform.* **3**, 33 (2011). https://doi.org/10.1186/1758-2946-3-33

33. Hanwell, M. D., Curtis, D. E., Lonie, D. C., Vandermeersch, T., Zurek, E. & Hutchison, G. R. Avogadro: an advanced semantic chemical editor, visualization, and analysis platform. *J. Cheminform.* **4**, 17 (2012). https://doi.org/10.1186/1758-2946-4-17

34. The Avogadro Team. Avogadro—free cross-platform molecular editor. https://avogadro.cc/ (accessed 29 December 2025).

35. Morris, G. M., Huey, R., Lindstrom, W., Sanner, M. F., Belew, R. K., Goodsell, D. S. & Olson, A. J. AutoDock4 and AutoDockTools4: automated docking with selective receptor flexibility. *J. Comput. Chem.* **30**, 2785–2791 (2009). https://doi.org/10.1002/jcc.21256

36. Cournia, Z., Allen, B. & Sherman, W. Relative binding free energy calculations in drug discovery: recent advances and practical considerations. *J. Chem. Inf. Model.* **57**, 2911–2937 (2017). https://doi.org/10.1021/acs.jcim.7b00564

37. Billah, M. M., Ahmed, M., Islam, M. Z. & Yamazaki, M. Processes and mechanisms underlying burst of giant unilamellar vesicles induced by antimicrobial peptides and compounds. *Biochim. Biophys. Acta Biomembr.* **1866**, 184330 (2024). https://doi.org/10.1016/j.bbamem.2024.184330

38. Bajpai, V. K., Sharma, A. & Baek, K. H. Antibacterial mode of action of *Cudrania tricuspidata* fruit essential oil, affecting membrane permeability and surface characteristics of food-borne pathogens. *Food Control* **32**, 582–590 (2013). https://doi.org/10.1016/j.foodcont.2013.01.032

39. Zhang, Y., Liu, X., Wang, Y., Jiang, P. & Quek, S. Antibacterial activity and mechanism of cinnamon essential oil against *Escherichia coli* and *Staphylococcus aureus*. *Food Control* **59**, 282–289 (2016). https://doi.org/10.1016/j.foodcont.2015.05.032

40. Xu, F., Xie, Y., Yu, W. & Wang, Z. Breaking the outer membrane barrier: structure, targets, and antimicrobial strategies for Gram-negative bacteria. *Front. Microbiol.* **17**, 1734749 (2026). https://doi.org/10.3389/fmicb.2026.1734749

41. Benfield, A. H. & Henriques, S. T. Mode-of-action of antimicrobial peptides: membrane disruption vs. intracellular mechanisms. *Front. Med. Technol.* **2**, 610997 (2020). https://doi.org/10.3389/fmedt.2020.610997

42. Lee, T. H., Charchar, P., Separovic, F., Reid, G. E., Yarovsky, I. & Aguilar, M. I. The intricate link between membrane lipid structure and composition and membrane structural properties in bacterial membranes. *Chem. Sci.* **15**, 3408–3427 (2024). https://doi.org/10.1039/D3SC04523D

43. Benaissa, A., Khadir, A., Tamfu, A. N., Kucukaydin, S., Latti, N., Benbelaïd, F., Boudiba, S., Eroglu, B., Bendahou, M. & Ceylan, O. Biofilm disruption and virulence attenuation effects of essential oil from endemic Algerian *Cistus munbyi* (Cistaceae) against clinical strains of *Pseudomonas aeruginosa*. *Nat. Prod. Commun.* **19**, 1934578X241245234 (2024). https://doi.org/10.1177/1934578X241245234

44. Flemming, H. C., van Hullebusch, E. D., Neu, T. R., Nielsen, P. H., Seviour, T., Stoodley, P., Wingender, J. & Wuertz, S. The biofilm matrix: multitasking in a shared space. *Nat. Rev. Microbiol.* **21**, 70–86 (2023). https://doi.org/10.1038/s41579-022-00791-0

45. Ahsan, A., Barnes, T. J. & Prestidge, C. A. Gentamicin–rhDNase liquid crystalline nanoparticles for pathogen-dependent antibiofilm activity against Gram-positive and

Gram-negative biofilms. *J. Drug Deliv. Sci. Technol.* (2026). https://doi.org/10.1016/j.jddst.2026.108972

46. Helcman, M., Šmejkal, K., Čulenová, M., Béres, T. & Treml, J. Natural phenolics disrupt microbial communication by inhibiting quorum sensing. *Microorganisms* **13**, 287 (2025). https://doi.org/10.3390/microorganisms13020287
47. Wen, F., Wu, Y., Yuan, Y., Yang, X., Ran, Q., Gan, X., Guo, Y., Wang, X., Chu, Y. & Zhao, K. Discovery of psoralen as a quorum sensing inhibitor suppresses *Pseudomonas aeruginosa* virulence. *Appl. Microbiol. Biotechnol.* **108**, 222 (2024). https://doi.org/10.1007/s00253-024-13067-9
48. Galiatsatos, P. et al. Psoralen: a narrative review of current and future therapeutic uses. *J. Cancer Res. Clin. Oncol.* **150**, 130 (2024). https://doi.org/10.1007/s00432-024-05648-y
49. Paczkowski, J. E., Mukherjee, S., McCready, A. R., Cong, J. P., Aquino, C. J., Kim, H., Henke, B. R., Smith, C. D. & Bassler, B. L. Flavonoids suppress *Pseudomonas aeruginosa* virulence through allosteric inhibition of quorum-sensing receptors. *J. Biol. Chem.* **292**, 4064–4076 (2017). https://doi.org/10.1074/jbc.M116.770552
50. Hernando-Amado, S., Alcalde-Rico, M., Gil-Gil, T., Valverde, J. R. & Martínez, J. L. Naringenin inhibition of the *Pseudomonas aeruginosa* quorum sensing response is based on its time-dependent competition with N-(3-oxo-dodecanoyl)-L-homoserine lactone for LasR binding. *Front. Mol. Biosci.* **7**, 25 (2020). https://doi.org/10.3389/fmolb.2020.00025

Supplementary Files

This is a list of supplementary files associated with this preprint. Click to download.

- Supplementaryinformation.docx